Test Results of Two ITER TF Conductor Short Samples Using High Current Density Nb_3Sn Strands

P. Bruzzone, M. Bagnasco, D. Ciazynski, A. della Corte, A. Di Zenobio, R. Herzog, Y. Ilyin, B. Lacroix, L. Muzzi, A. Nijhuis, B. Renard, E. Salpietro, L. S. Richard, B. Stepanov, S. Turtù, A. Vostner, R. Wesche, L. Zani, and R. Zanino

***Abstract*—Two short length samples have been prepared and tested in SULTAN to benchmark the performance of high current density, advanced Nb_3Sn strands in the large cable-in-conduit conductors (CICC) for ITER. The cable pattern and jacket layout were identical to the Toroidal Field Model Coil Conductor (TFMC), tested in 1999. The four conductor sections used strands from OST, EAS, OKSC and OCSI respectively. The Cu:non-Cu ratio was 1 for three of the new strands, compared to 1.5 in the TFMC strand. The conductors with OST and OKSC strands had one Cu wire for two Nb_3Sn strands, as in TFMC. In the EAS and OCSI conductors, all the 1080 strands in the cable were Nb_3Sn. A dc test under relevant load conditions and a thermal-hydraulic campaign was carried out in SULTAN. The CICC performance was strongly degraded compared to the strand for all the four conductors. The current sharing temperature at the ITER TF operating conditions ($j_{op} = 286$ A/mm^2, $B = 11.15$ T) was lower than requested by ITER.**

***Index Terms*—Cable-in-conduit conductor, ITER, Nb_3Sn strand.**

I. Introduction

THE conductor development for ITER from 1993 to 1999 led to a number of tests on short sample conductors and model coils, whose performance was not satisfactory for the ITER requirements [1]. In an update of the ITER conductor design [2], the cross section of the Nb_3Sn superconductor was increased and the specification of the strand critical current was raised according to the improved performance obtained, for example, in the production of Nb_3Sn strand for the KSTAR project [3].

Manuscript received August 28, 2006.

P. Bruzzone, R. Herzog, B. Stepanov, and R. Wesche are with EPFL-CRPP, Fusion Technology, 5232 Villigen PSI, Switzerland (e-mail: pierluigi.bruzzone@psi.ch; robert.herzog@psi.ch; boris.stepanov@psi.ch; rainer.wesche@psi.ch).

M. Bagnasco. L. S. Richard, and R. Zanino are with Politecnico, 10129 Torino Italy (e-mail: maurizio.bagnasco@polito.it; laura.savoldi@polito.it; roberto.zanino@polito.it).

D. Ciazynski, J.-L. Duchateau, B. Renard, and L. Zani are with CEA Cadarache, 13108 St. Paul Lez Durance, France (e-mail: daniel.ciazynski@cea.fr; benoit.lacroix@cea.fr; bertrand.renard@cea.fr; louis.zani@cae.fr).

A. della Corte, A. Di Zenobio, L. Muzzi, and S. Turtù are with ENEA, 00044 Frascati, Italy (e-mail: dellacorte@frascati.enea.it; dizenobio@frascati.enea.it; muzzi@frascati.enea.it; turtu@frascati.enea.it).

Y. Ilyin and A. Nijhuis are with University of Twente, 7500 AE Enschede, The Netherlands (e-mail: Y.Ilyin@tnw.utwente.nl; A.Nijhuis@tnw.utwente.nl).

E. Salpietro and A. Vostner are with EFDA, 85748 Garching b. München, Germany (e-mail: ettore.salpietro@tech.efda.org; alexander.vostner@tech.efda.org).

Digital Object Identifier 10.1109/TASC.2007.898504

TABLE I
STRAND CHARACTERISTICS

	OST	EAS	OKSC	OCSI
Strand diameter (Cr coated), mm		0.81		
Cu:non-Cu	1.05	0.92	1.05	1.45
Manufacturing technology	Int Sn	Bronze	Int Sn	Int Sn
Diffusion barrier	Ta	Ta	Ta	NbTa
Non-Cu hysteresis loss ± 3 T, kJ/m^3	700	200	1000	1000
J_c@4.2 K, 12 T, 10 μV/m, A/mm^2 [A]	1100	780	1000	950
J_c@4.2 K, 12 T, 10 μV/m, A/mm^2 [B]	1068	705[C]	999	1001
n – index @ 12 T, 4.2 K	34	41	16	15

[A] data provided by the supplier
[B] test results from witness strands, average of three specimens
[C] the heat treatment for TFAS1 is not optimized for EAS strand

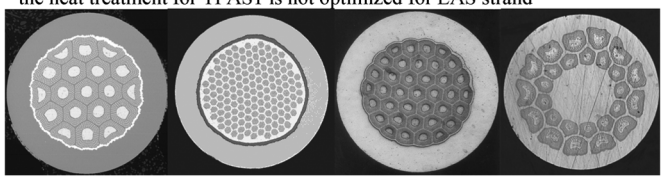

OST EAS OKSC OCSI

An R&D program was launched in Europe in 2003 to qualify the use of high current density Nb_3Sn strands in ITER cable-in-conduit conductors [4]. The program was completed in spring 2006 with the test in SULTAN of two conductor short samples (ITER-TFMC layout), using strands from four different suppliers. The test results are discussed below.

II. Strands, Conductor and Sample Layout

From the six R&D contracts launched in 2003 [4], four types of Nb_3Sn strand were successfully qualified and selected for the manufacture of four CICC sections. In Table I the strands are identified with the short name of the supplier: OST for Oxford Instruments, EAS for European Advanced Superconductors, OKSC for Luvata Pori and OCSI for Luvata Italy. The j_c result at 4.2 K and 12 T is given both as certified by the supplier and as measured on witness samples (ITER barrels) heat-treated together with the CICC sections.

From the 4 types of strand, four CICCs were manufactured at OCSI to the same specification as the Toroidal Field Model Coil (TFMC) conductor [5]. The four CICCs were assembled into two SULTAN samples, named respectively TFAS1 and TFAS2, with layout substantially identical to the TFMC sample [6]. Copper segregation, i.e. replacing one Nb_3Sn strand by a copper wire in the first triplet, was used in the right leg (R) of both samples, see Table II, with the aim to obtain similar critical current in both legs of the same sample.

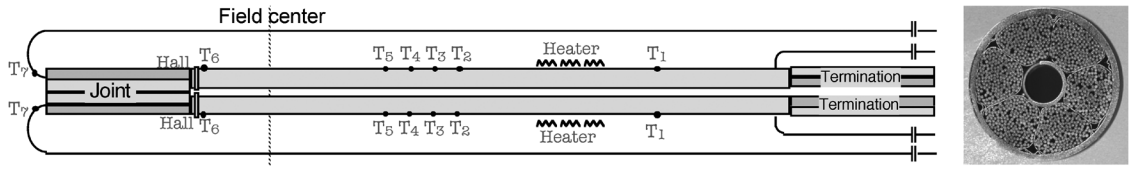

Fig. 1. Instrumentation sketch of a TFAS sample. The flow inlet is at the joint for TFAS2 (bottom-to-top) and at the termination for TFAS1 (top-to-bottom).

TABLE II
CONDUCTORS AND SAMPLES CHARACTERISTICS

	OST	EAS	OKSC	OCSI
	TFAS1-R	TFAS1-L	TFAS2-R	TFAS2-L
Steel jacket, od/id, mm	40.4 / 37.2			
Steel spiral, od/id, mm	12 / 10			
Twist pitch sequence, mm	45 / 87 / 126 / 166 / 415			
Void fraction, %	32.7	33.9	33.5	32.5
# of sc strands	720	1080	720	1080
# of copper wires	360	0	360	0
Total non-Cu cross section, mm^2	181	290	181	227
Heat treatment schedule, °C/h	210/50+340/25+450/ 25+575/100+660/100		185/24 + 460/48 + 575/100 + 650/175	

The heat treatment was carried out at CRPP in a vacuum furnace with purging Ar gas inside the conductors. The TFAS sample size is the standard size of the SULTAN samples [7], about 3.5 m long. The two conductor lengths were cooled in parallel by two circuits with independent regulation of temperature (SULTAN heaters) and mass flow. For TFAS1, the coolant flows downward from the termination to the joint. In the TFAS2 dc test, the flow was upward from bottom to top, with the central channel plugged in the joint region.

The sample instrumentation, Fig. 1, included one array of six Hall sensors next to the joint, one heater and seven temperature sensors on each leg. In the first test campaign of TFAS1, the response of the temperature sensors was not satisfactory (poor thermalization of the sensor leads). Then the sensors at T6 and T5 were duplicated and eventually the readout of the new T5 sensors is retained. For TFAS2, all sensors except T1, had correct readout. In both samples, the readout of T6, next to the joint, was not fully reliable with transport current, due to azimuthal temperature gradients and, for TFAS1, buoyancy perturbations from the joint.

The test program was focused on dc test. For TFAS2 a thermal-hydraulic test was also carried out, with the central channel free and downward flow to investigate heat exchange between the central channel and the strand bundle using the heaters wrapped on the jacket, see Fig. 1. The dc test included $\mathrm{T_{cs}}$ and $\mathrm{I_c}$ runs at 8, 9, 10 and 11 T background field. To avoid transverse load in excess of the ITER operation loads, the product field-current was always limited to $\mathrm{BI} \leq 770\ \mathrm{kA \cdot T}$. After a first campaign of dc test, cyclic load was applied 1000 times for TFAS1 and 800 times for TFAS2 by raising the current to 0-70-0 kA in a background field of 11 T and the dc test was repeated. The performance evolution was monitored by a bench mark $\mathrm{T_{cs}}$ test, periodically carried out at 11 T.

TABLE III
STRAND SCALING PARAMETERS

	OST	EAS	OKSC	OCSI
p	0.9631	0.4625	0.4556	0.8869
q	2.229	1.452	1.723	2.174
n^*	2.532	2.457	2.642	2.500
ν	1.518	1.225	1.318	1.500
w	2.423	2.216	2.430	2.200
u	0.1155	0.051	-0.811	0
$A(\varepsilon=0)$, $Am^{-2}T^{3-n^*}K^{-2}$	$3.86\cdot10^7$	$1.48\cdot10^7$	$1.26\cdot10^7$	$2.87\cdot10^7$
$T_c^*(\varepsilon=0)$, K	16.71	17.58	17.22	17.50
$B_{c2}^*(T=0,\ \varepsilon=0)$, T	29.72	29.59	29.41	28.47
c_2	-0.7816	-0.6602	-1.0768	-0.7392
c_3	-0.6318	-0.4656	-1.1514	-0.5071
c_4	-0.1732	-0.1075	-0.4125	-0.0838
$\varepsilon_{\mathrm{Barrel}}$, %	-0.14	-0.22	-0.095	-0.07

III. SUMMARY OF TEST RESULTS

A. Strand Scaling and CICC Performance Prediction

The scaling formulae proposed by D. Hampshire [8] were used to scale the strand performance as a function of the operating temperature, field and longitudinal strain.

$$J_e(B,T,\varepsilon)=A(\varepsilon)\left[T_c^*(\varepsilon)(1-t^2)\right]^2\cdot\left[B_{c2}^*(T,\varepsilon)\right]^{n^*-3}b^{p-1}(1-b)^q \tag{1}$$

$$B_{c2}^*(T,\varepsilon)=B_{c2}^*(0,\varepsilon)(1-t^\nu) \tag{2}$$

$$\left(\frac{A(\varepsilon)}{A(0)}\right)^{w/u}=\left(\frac{T_c^*(\varepsilon)}{T_c^*(0)}\right)^w=\frac{B_{c2}^*(0,\varepsilon)}{B_{c2}^*(0,0)}=1+c_2\varepsilon^2+c_3\varepsilon^3+c_4\varepsilon \tag{3}$$

The scaling parameters for the four strands are listed in Table III, where the A(0) parameter is adjusted to match the results of the witness strands at 4.2 K, 12 T. The retained strain for the witness strands, $\varepsilon_{\mathrm{Barrel}}$ is also listed in Table III.

Based on the data of Tables I, II and III, the 10 μV/m $\mathrm{T_{cs}}$ performance of the CICC at 11 T, 70 kA was calculated for a thermal strain $\varepsilon = -0.61\%$ (relaxed fully bonded model [2]) and the same n index as in the strand, i.e. no degradation.

Other "free" predictions were done by the testing group at the same operation point, leaving the analysts free to choose ε/n and include degradation. The CEA prediction used an effective strain which is a function of the BI product, as from the TFMC results assessment [9], and a reduced n index. CEA also included the effect of the strand/field angle in the cable. This prediction was the bench mark to straight compare the TFAS and TFMC conductors. The "free" prediction of CRPP maintained the thermal strain $\varepsilon = -0.61\%$ and a reduced n index in the CICC as well as a reduction of the effective non-Cu area to account for degradation: -10% for OST and -30% for EAS, OKSC and OCSI. These values are drawn from an assessment of subsize conductors made of similar strands [10], [11]. Polito's

TABLE IV
T_{cs} PERFORMANCE PREDICTIONS AT 70 kA, 11 T

	OST TFAS1-R	EAS TFAS1-L	OKSC TFAS2-R	OCSI TFAS2-L
Non-Cu J at 70 kA, A/mm^2	386	241	386	308
T_{cs} @ ε_{th} = -0.61 %, K	6.15	6.59	5.46	6.45
CEA free Prediction, K	5.78	6.26	5.10	6.96
CRPP free Prediction, K	5.83	5.7	4.45	5.62
Polito free Prediction, K	5.34	5.84	3.92	4.61

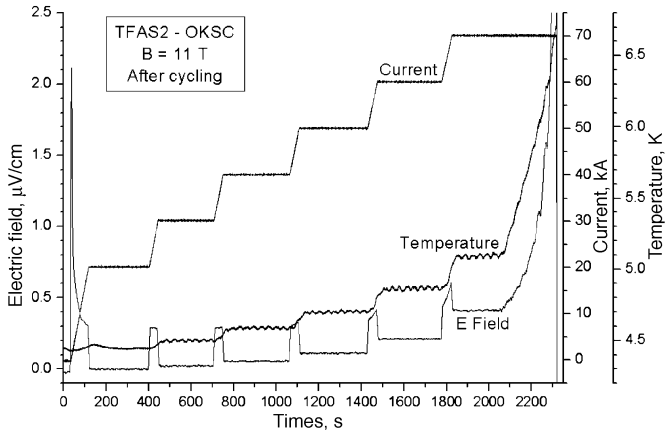

Fig. 2. An example of broad transition. The current is raised in steps of 10 kA and the temperature is eventually raised till a quench occur at 70 kA/6.6 K. The T_{cs} criterion is already largely exceeded at 60 kA, 4.8 K.

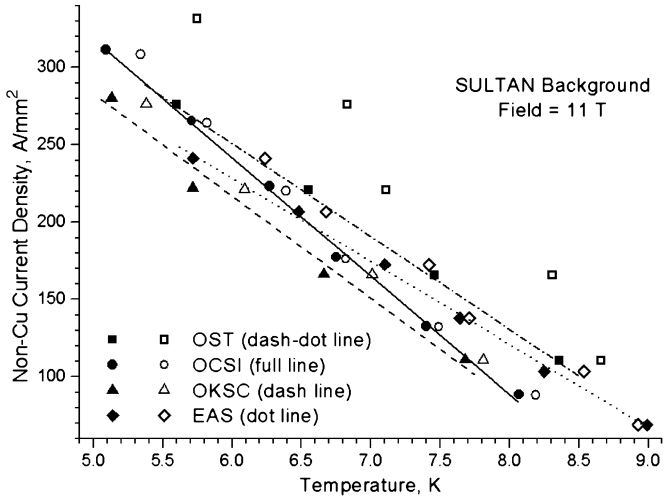

Fig. 3. Summary of T_{cs} data at 11 T SULTAN field before (open symbols) and after cyclic load (full symbols). Trend lines are drawn for the data after cyclic loading.

TABLE V
T_{cs} PERFORMANCE SCALED TO ITER TF OPERATION, 286 A/mm^2, 11.15 T

	ITER spec	TFMC	OST	EAS	OKSC	OCSI
Before cyclic load	5.7 K	5.52 K	6.63 K	4.93 K	5.29 K	5.77 K
After cyclic load	5.7 K	-	5.81 K	4.72 K	5.09 K	5.53 K
After re-installation	5.7 K	-	5.44 K	4.57 K	-	-

"free" prediction for EAS and OST used the effective strain as in [9]. For OKSC and OCSI, Polito retained the effective strain deduced from the results of TFAS1-EAS. All prediction results are gathered in Table IV.

B. DC Test Before and After Cyclic Load

A common feature to the four conductors of TFAS samples was a very broad transition, with the quench point (I_q or T_q), far away from I_c or T_{cs}, see Fig. 2. Furthermore, a voltage (either positive or negative) proportional to the current was observed since very low current, varying with the position of the voltage taps, the background field and the loading history. Although the nature of this "linear voltage" is not fully understood, it was arbitrarily subtracted to process the data. Only the deviation from the linear voltage was considered evidence of current sharing. The very low slope of the electric field vs. temperature or current (low n index) and the procedure of voltage compensation affected the accuracy of the data reduction with an error bar of ± 0.15 K.

The dc results (T_{cs} and I_c runs) were collected at background fields of 8, 9, 10 and 11 T, in the range of operating current up to 80 kA and temperature from 4.5 K to about 9 K. As the four conductors have different non-Cu cross sections, the results at 11 T background field are better presented in Fig. 3 as critical current density vs. temperature before and after cyclic load. Most of the performance evolution under cyclic load was observed in the first 100 cycles. The OST conductor lost up to 1 K during cyclic load. The data before cyclic loading are not collected strictly sequentially for OST and EAS, producing an impression of large scattering in Fig. 3, which is evidence of the ongoing performance degradation observed during operation on these conductors. The n index was in the range of 4–8 for all the conductors, without substantial change upon cyclic load. The lowest value was observed for the OKSC.

The ITER TF conductors operate at $J_{op} = 286$ A/mm^2 and $B = 11.15$ T (average over the conductor cross section). In the TFAS samples at background field 11 T and $J_{op} = 286$ A/mm^2, the average field over the conductor cross section was 11.21 T for OST and OKSC, 11.26 T for OCSI and 11.33 T for EAS. The T_{cs} performance of the EAS, OKSC and OCSI conductors at the ITER operating conditions is interpolated from Fig. 3 and marginally corrected for 11.15 T average field. The results before and after cyclic load are gathered in Table V, including also the performance of the TFMC conductor [12].

C. Analysis of DC Results

The results analysis was restricted to the T_{cs} data measured at 11 T after cyclic loading. All the approaches retain the strand scaling laws quoted above and a balanced current distribution among the strands, without inter-strand current sharing.

The first approach lets the ε of the scaling laws vary to fit the results. The average of the background field and self-field over the conductor cross section is retained. The fit is done on the point at 10 μV/m, i.e. the change of n index and the slope of the V(T) curve is disregarded. Two parameters, ε_{th} and γ, make up the total ε fitting the results, $\varepsilon = \varepsilon_{th} - \gamma \cdot BI$, where I (kA) is the operating current and B (T) is the average field over the conductor. For each conductor, the set of parameters and the standard deviation, σ, are reported in Table VI.

A second approach uses a constant ε and a filament area reduced by a factor f to fit the results [10]. For each conductor, both ε and f are optimized applying the least square criterion to the set of T_{cs} results. The voltage over one strand of the CICC is calculated as the integral of the local electric field along the

TABLE VI
ANALYSIS OF DATA AT 11 T BACKGROUND FIELD, AFTER CYCLIC LOAD

		OST	EAS	OKSC	OCSI
First approach $\varepsilon = \varepsilon_{th} - \gamma(BI)$	ε_{th}, %	-0.54	-0.51	-0.56	-0.68
	γ, % $kA^{-1}T^{-1}$	0.00052	0.00036	0.00054	0.00019
	σ, %	n.a.	1.6	7.0	1.1
Second approach	f	0.35	0.50	0.45	0.70
	ε, %	-0.35	-0.42	-0.48	-0.66
	n index	6	7	5	n^{strand}
Mixed approach	ε_{th}, %	-0.53	-0.51	-0.55	-0.65
	γ, % $kA^{-1}T^{-1}$	0.00040	0.00033	0.00030	0.00005
	f	0.80	0.95	0.72	0.72

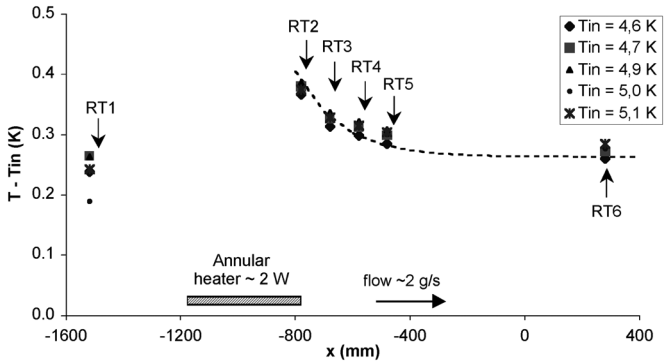

Fig. 4. Distributions of temperature difference $\mathrm{T(x)} - \mathrm{T_{in}}$ along TFAS2 right leg, for 5 inlet temperatures. The RT1 sensor, even after re-calibration, did not properly respond.

path of a transposed strand in the cable. The retained n index for the strand is lowered according to the CICC results. As the original strand and CICC have different n index, the result of the analysis is a function of the electric field criterion retained for the data reduction.

In a mixed approach, both variable ε and f, are applied. The "effective" field retained for the scaling law is lower than the peak field and slightly higher than the average field and is calculated by a self-field factor $k = 5.2 \cdot 10^{-3}$ T/kA, $B_{\text{eff}} = B_{\text{background}} + kI_{\text{op}}$. The k factor corresponds to a B_{eff} computed from best fits of the V(T) curves with an average $n = 5$. The electric field E is computed by an averaging of $E(\mathrm{x}, \mathrm{y})$ across the cable cross-section.

D. Thermal-Hydraulic Test of TFAS2

Thermal-hydraulic tests on TFAS2 were aimed to investigate the heat exchange coefficient H between central and strand bundle channels. The sample was tested with downward flow and free central channel. A first method to assess H is based on steady state heating by jacket annular heaters, see Fig. 1, and aims to measure the characteristic length Λ [13]. Fig. 4 shows the temperature distribution along the right leg, with 2 g/s mass flow and 2 W heat deposition. The thermal behavior and thus the heat exchange coefficient are not significantly affected by the inlet temperature. A second method leans on the transient response to an inlet temperature step, inducing the propagation of the temperature front in both channels [14], allowing an independent assessment of H.

IV. CONCLUSION

The expected improvement of the cable-in-conduit performance using Nb_3Sn strand with high current density could not be achieved in the TFAS conductors. Performance predictions based on the TFMC conductor without cyclic load were not adequate for the TFAS conductors.

At the ITER non-Cu operating current and field, $\mathrm{J_{op}} = 286$ A/mm^2 and $\mathrm{B} = 11.15$ T, the current sharing temperature was below 5.7 K for all four TFAS conductors, in particular the EAS one made of standard bronze strand fulfilling the present ITER TF bronze strand specification.

The very low n index as well as early, linear voltages, affected the accuracy of the measurements, with a likely error bar of ± 0.15 K on the $\mathrm{T_{cs}}$ results.

The substantial degradation of the performance under cyclic load, mostly for OST conductor, suggests that the degradation is due to the operating load rather than to accidental damage.

The analysis, both with "extra strain" and reduced filament cross section, did not provide a satisfactory, overall picture, with the fitting parameters broadly varying among the four conductors and, within the same conductor, according to the results, either high or low field.

The thermal-hydraulic tests provided a data base for the assessment of the heat exchange coefficient between annular and central channels, under stationary and transient conditions.

ACKNOWLEDGMENT

The technical support of PSI in the experimental activity is acknowledged.

REFERENCES

[1] N. Mitchell, "Summary, assessment and implication of the ITER model coil test results," *Fusion Engineering and Design*, vol. 66–68, pp. 971–993, 2003.
[2] "ITER Final Design Report," IAEA Vienna and ITER IT team Design Description Document 1.1 Update, January 2004.
[3] M. Kim *et al.*, "The results of performance test of superconducting wires for KSTAR magnets," *Adv. Cryog. Eng.*, vol. 48, pp. 994–1000, 2002.
[4] A. Vostner and E. Salpietro, "The European Nb_3Sn advanced strand development program," *Fusion Eng. and Design*, vol. 75–79, pp. 169–172, 2005.
[5] A. della Corte *et al.*, "Successful completion of the conductor manufacture for the ITER TF Model Coil," in *Fusion Technology 1998, Proc. of SOFT 20th*, September 1998, pp. 841–844.
[6] D. Ciazynski *et al.*, "Fabrication of the first European full size joint sample for ITER TFMC," *IEEE Appl. Supercon.*, vol. 9, pp. 648–651, 1999.
[7] "User Specification for Conductor samples to be tested in the SULTAN Facility," CRPP LRP 723/02, June 2002.
[8] D. M. Taylor and D. P. Hampshire, "The scaling law for the strain dependance of the critical current density in Nb_3Sn superconducting wires," *Supercond. Sci. Technol.*, vol. 18, pp. 241–252, 2005.
[9] R. Zanino *et al.*, "Coupled mechanical-electromagnetic-thermal-hydraulic effects in Nb_3Sn cable-in-conduit conductors for ITER," *Supercond. Sci. Technol.*, vol. 18, pp. 376–382, 2005.
[10] P. Bruzzone, B. Stepanov, and R. Wesche, "Transverse load degradation in Nb_3Sn cable-in-conduit conductors with different cable pattern," *Adv. Cryog. Eng.*, vol. 52 B, pp. 558–565, 2006.
[11] P. Bruzzone *et al.*, "Test results of a small size CICC with advanced Nb_3Sn strands," *IEEE Trans. Appl. Supercon.*, vol. 16, pp. 894–897, 2006.
[12] D. Ciazynski *et al.*, "Test results and analysis of two European full size conductor samples for ITER," *IEEE Appl. Supercon.*, vol. 10, pp. 1058–1061, 2000.
[13] S. Nicollet *et al.*, "Evaluation of the ITER cable-in-conduit-conductor heat transfer," in *Proc. of ICEC 20*, Beijing, China, 2004, pp. 589–592.
[14] B. Renard *et al.*, "Transverse heat transfer coefficients on a full size dual channel CICC ITER conductor," *Cryogenics*, vol. 46, pp. 530–540, 2006.